molecular pharmaceutics

Article

pubs.acs.org/molecularpharmaceutics

Reformulating Tylocrebrine in Epidermal Growth Factor Receptor Targeted Polymeric Nanoparticles Improves Its Therapeutic Index

Ameya R. Kirtane,[†] Henry L. Wong,[‡,§] Bharath Raja Guru,[†] Lev G. Lis,[‡,§] Gunda I. Georg,[‡,§,⊥] Vadim J. Gurvich,[‡,§,⊥] and Jayanth Panyam*[,†,⊥]

[†]Department of Pharmaceutics, [‡]Institute of Therapeutics Discovery and Development, [§]Department of Medicinal Chemistry, and [⊥]Masonic Cancer Center, University of Minnesota, Minneapolis, Minnesota 55455, United States

Supporting Information

ABSTRACT: Several promising anticancer drug candidates have been sidelined owing to their poor physicochemical properties or unfavorable pharmacokinetics, resulting in high overall cost of drug discovery and development. Use of alternative formulation strategies that alleviate these issues can help advance new molecules to the clinic at a significantly lower cost. Tylocrebrine is a natural product with potent anticancer activity. Its clinical trial was discontinued following the discovery of severe central nervous system toxicities. To improve the safety and potency of tylocrebrine, we formulated the drug in polymeric nanoparticles targeted to the epidermal growth factor receptor (EGFR) overexpressed on several types of tumors. Through *in vitro* studies in different cancer cell lines, we found that EGFR targeted nanoparticles were significantly more effective in killing tumor cells than the free drug. *In vivo* pharmacokinetic studies revealed that encapsulation in nanoparticles resulted in lower brain penetration and enhanced tumor accumulation of the drug. Further, targeted nanoparticles were characterized by significantly enhanced tumor growth inhibitory activity in a mouse xenograft model of epidermoid cancer. These results suggest that the therapeutic index of drugs that were previously considered unusable could be significantly improved by reformulation. Application of novel formulation strategies to previously abandoned drugs provides an opportunity to advance new molecules to the clinic at a lower cost. This can significantly increase the repertoire of treatment options available to cancer patients.

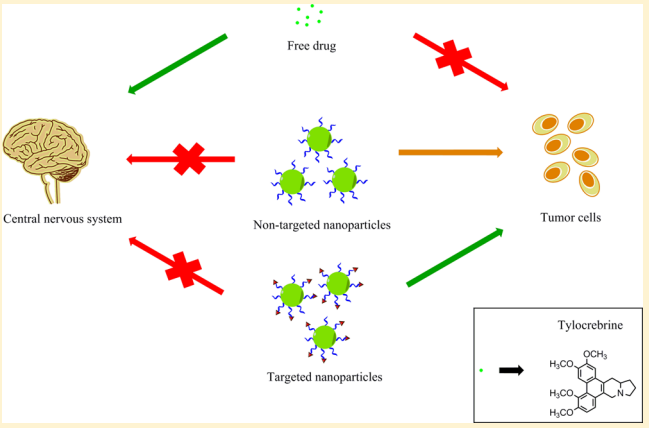

KEYWORDS: *tylocrebrine, PLGA nanoparticles, drug targeting, therapeutic index, chemotherapy*

INTRODUCTION

Much of current cancer research is focused on exploring novel targets and discovering new anticancer drugs. While the availability of new molecules certainly offers hope to patients who do not respond to existing drugs, development of each new molecule is associated with tremendous costs.[1,2] Many highly active drug candidates have been shelved because of poor physicochemical or pharmacokinetic characteristics.[3−5] Reformulation of such molecules can overcome their unfavorable biological behavior and would offer a less expensive approach to anticancer drug development.[4,6,7]

Tylocrebrine, a phenanthropiperidine alkaloid, is an example of a drug with potent anticancer activity and whose clinical trial was discontinued following the discovery of severe central nervous system (CNS) toxicities. The CNS toxicities of the drug were likely caused by its extensive penetration into the brain.[8,9] We hypothesized that encapsulation of tylocrebrine in poly(lactide-*co*-glycolide) (PLGA)-based polymeric nanoparticles will limit the distribution of the drug to the CNS, potentially decreasing its neurological toxicities. Additionally, nanoparticles are known to passively accumulate in the tumor tissue through the enhanced permeability and retention (EPR) effect.[10,11] The combination of these properties should result in significantly improved therapeutic index. To further enhance the tumor cell uptake and retention of nanoparticles, we functionalized the nanoparticle surface with a peptide capable of targeting the epidermal growth factor receptor (EGFR),[12,13] which is overexpressed on the cell membrane of multiple solid tumors.[14] Using *in vitro* and *in vivo* models of EGFR-overexpressing tumors, we evaluated the therapeutic benefit of encapsulating tylocrebrine in nanoparticles. Our studies show that this reformulation strategy significantly improved the antitumor efficacy while reducing the brain penetration of tylocrebrine.

MATERIALS AND METHODS

Materials. Amine-terminated poly(ethylene glycol) (molecular weight 3400 Da) was purchased from Laysan Bio Inc. (Arab, AL).

Received: February 26, 2015
Revised: May 22, 2015
Accepted: June 11, 2015
Published: June 11, 2015

DOI: 10.1021/acs.molpharmaceut.5b00173
Mol. Pharmaceutics 2015, 12, 2912−2923

PLGA (50:50 molar ratio of lactide−glycolide, molecular weight ∼40 kDa) was purchased from Lactel (Birmingham, AL). Poly(vinyl alcohol) (molecular weight 30−70 kDa) and lactic acid were obtained from Sigma-Aldrich Co. (St. Louis, MO). EGFR-targeting peptide (YHWYGYTPQNVI) and scrambled peptide (HWPYAHPTHPSW) were obtained from Peptide 2.0, Inc. (Chantilly, VA). Radioimmunoprecipiation (RIPA) buffer and bicinchoninic acid assay kit were obtained from Thermo Scientific (Rockford, IL). All other chemicals were obtained from Sigma-Aldrich Co. (St. Louis, MO). Tylocrebrine was synthesized as described previously.[15]

Cell Culture. A549 human lung cancer cell line was obtained from ATCC. A431 human epidermoid cancer cells were obtained from Dr. Benjamin Hackel (University of Minnesota). A549 cells were cultured in Dulbecco's minimum essential media (DMEM), while A431 cells were grown in Roswell Park Memorial Institute media (RPMI-1640). Both media were supplemented with 10% v/v fetal bovine serum and 1% v/v penicillin−streptomycin. The cells were grown in a humidified environment consisting of 5% CO_2/95% air and were maintained at 37 °C.

Effect of Extracellular pH on Cell Uptake of Tylocrebrine. We determined the effect of extracellular pH on the cell accumulation of tylocrebrine. For low pH conditions, serum-free RPMI was acidified with 9.1% v/v 0.1 M HCl. The pH of acidified RPMI was maintained between 6.3 and 6.7 for 6 h when placed under routine cell culture conditions.

Aliquots of 5 ×10^4 A431 cells were seeded in a 24-well plate and allowed to adhere overnight. Tylocrebrine was first dissolved in 1 M HCl (1:1 molar ratio) and then diluted in serum-free RPMI to prepare a stock solution of 1 mg/mL. The stock solution was then diluted to 5 μg/mL in neutral or acidic serum-free RPMI and added to the cells. Treatments were removed 1 h later, and the cells were washed with cold 1X phosphate buffered saline (PBS). Cells were digested with RIPA buffer (0.1 mL) for 15 min, and the cell lysate was divided into two parts. One part (20 μL) was analyzed by bicinchoninic acid assay (BCA) to determine cell protein concentration (ELx800 absorbance microplate reader, Biotek Inc., Winooski, VT). The other part (80 μL) was extracted overnight with methanol and tylocrebrine concentration in the methanol extract and was analyzed using high-performance liquid chromatography (HPLC). HPLC was performed on a Beckman Coulter HPLC system equipped with a System Gold 508 autosampler. A Beckman Coulter C18 column (4.6 mm × 250 mm, 5 μm) was used as the stationary phase. The mobile phase consisted of 80:20 mix of acetonitrile and 87 mM ammonium acetate (pH 4.2), run isocratically at a flow rate of 1 mL/min. Tylocrebrine was analyzed by measuring absorbance at 265 nm using a System Gold UV detector.

Synthesis of Carboxyl Terminated Block Copolymer of Poly(lactide) and Poly(ethylene glycol). A block copolymer of poly(lactide) (PLA) and carboxyl-terminated poly(ethylene glycol) (PEG-COOH) was synthesized in a two-step process. In the first step, lactic acid was reacted with amine-terminated PEG to generate an amine-terminated block copolymer (PLA−PEG-NH_2).[16] In the second step, the terminal amino group was reacted with succinic anhydride to produce PLA−PEG-COOH.[13]

All glassware was rinsed with toluene and dried overnight at 100 °C prior to both reactions. For step one, amine-terminated PEG (400−500 mg) was dissolved in ∼80 mL of dichloromethane and added to a round-bottom flask. The mixture was stirred in the presence of N_2 gas for 10 min. Lactic acid (2 g) was added to this mixture and stirred for 10 min. About 20 μL of 1,8-diazabicyclo[5,4,0]undec-7-ene was added as a catalyst, and the reaction was allowed to proceed for 1 h. After 1 h, the solvent was reduced to ∼20 mL using a rotovap. The solution was added dropwise to chilled diethyl ether to precipitate the amine terminated block copolymer. The suspension was filtered, and the solid was dried at 25 °C in a vacuum oven. The product was dissolved in deuterated chloroform and characterized using ^{1}H NMR (Varian 400 MHz).

For step two, the amine terminated block copolymer (1 g) was dissolved in 50 mL of tetrahydrofuran and 5 mL of triethyl amine in a round-bottom flask. The mixture was stirred under N_2 gas for 10 min. Succinic anhydride (molar ratio of succinic anhydride to block copolymer was 1.1:1) was added to this solution. The reaction was allowed to proceed at 50 °C for 2 h. The reaction mixture was then concentrated using a rotavap and added to cold diethyl ether to precipitate the polymer. The polymer was filtered and dried in a vacuum oven at 25 °C. The product was dissolved in deuterated chloroform and characterized by ^{1}H NMR.

Synthesis, Optimization, and Physicochemical Characterization of Nanoparticles. PLGA nanoparticles loaded with tylocrebrine and surface functionalized with carboxyl-terminated PEG were synthesized by the interfacial activity assisted surface functionalization technique developed by our lab.[17,18]

Briefly, PLGA (30−35 mg) and tylocrebrine (5 mg) were dissolved in 1 mL of chloroform. An aqueous solution of 2% w/v poly(vinyl alcohol) in PBS (0.15 mM, pH 7.4; henceforth referred to as 1X PBS) was prepared. The polymer−drug mixture was added to the aqueous surfactant to form an o/w emulsion. The emulsion was probe sonicated at an output of 18−21 W for 5 min over an ice bath (Sonicator XL, Misonix, NY) and then stirred at 650 rpm on a magnetic stir plate. PLA−PEG-COOH (8 mg) dissolved in 0.2 mL of chloroform was added dropwise to the emulsion. The organic solvent was evaporated overnight under ambient conditions and then for 2 h under vacuum. The nanoparticle dispersion was washed twice with 30 mL of 1X PBS by ultracentrifugation (35 000 rpm, 35 min, 4 °C) (Beckman, Palo Alto, CA). After the second wash, nanoparticles were dispersed in 1.5 mL of 1X PBS. To this dispersion, 0.7 mg of *N*-hydroxysuccinimide (NHS), 1.14 mg of 1-ethyl-3-[3-(dimethylamino)propyl] carbodiimide hydrochloride (EDC), and 1.8 mg of targeting or control peptide were added, and the reaction was allowed to proceed for 3, 5, or 8 h. Following the conjugation reaction, nanoparticles were dispersed in 30 mL of deionized water and centrifuged (35 000 rpm, 35 min, 4 °C) to remove unconjugated peptide. The nanoparticle pellet was redispersed in ∼10 mL of deionized water, frozen below −50 °C for 2 h, and lyophilized (Labconco FreeZone 4.5, Kansas city, MO). The lyophilized formulation was stored at −20 °C.

To determine particle size and zeta potential, a dispersion of nanoparticles (∼1 mg/mL) was analyzed by dynamic light scattering (Delsa Nano C, Beckman Coulter, Fullerton, CA).

To determine drug loading, nanoparticles were dispersed in a mixture of methanol and acetic acid (95:5 v/v). Drug was extracted overnight at room temperature. Nanoparticles were separated from the extract by centrifugation (14 000 rpm, 15 min, 4 °C). The supernatant was analyzed by HPLC.

The amount of peptide on the surface of nanoparticles was determined using BCA. Nanoparticles were dispersed in deionized water and incubated with the BCA reagent for 20 min at 37 °C. The nanoparticle dispersion and standards were then centrifuged (14 000 rpm, 15 min, 25 °C), and the absorbance of

DOI: 10.1021/acs.molpharmaceut.5b00173
Mol. Pharmaceutics 2015, 12, 2912−2923

the supernatant was measured at 562 nm (ELx800 absorbance microplate reader, Biotek Inc., Winooski, VT).

Drug release kinetics was assessed in pH 7.4 and 6.5 buffers. Nanoparticles were dispersed in a sufficient volume of 1X PBS (pH 7.4 or 6.5) to maintain sink conditions. The dispersions were kept on a shaker at 37 °C and 100 rpm [C24 incubator shaker, New Brunswick Scientific (now Eppendorf Inc. Enfield, CT)]. At various time points, the released drug was separated from nanoparticles using a MicroKros filter module (Spectrum Laboratories, Rancho Dominguez, CA). The nanoparticle concentrate was retrieved and redispersed in the buffer. Drug solution was lyophilized, dissolved in a mixture of methanol and acetic acid (95:5 v/v), and analyzed by HPLC.

Cellular Uptake of EGFR-Targeted and Nontargeted Nanoparticles. We first determined whether cellular uptake of EGFR-targeted nanoparticles was higher than nontargeted nanoparticles and if their uptake was mediated by EGFR. A549 cells were seeded in a 24-well plate at a seeding density of 5×10^4 cells/well and allowed to adhere overnight. On the next day, nanoparticles loaded with a fluorescent dye (coumarin 6), in the presence or absence of excess free targeting peptide, were added to the cells. Cells were incubated with the treatments at 4 °C for 1 h, washed twice with 1X PBS, and incubated with fresh media at 37 °C. After 1 h, the media was aspirated, cells were washed with 1X PBS, and lysed with RIPA buffer. One part of the lysed cells was extracted with methanol, and coumarin 6 content was determined using HPLC.[18] The other part was analyzed by BCA assay to determine the amount of cell protein.

We also compared the cell uptake of targeted and nontargeted nanoparticles loaded with tylocrebrine. A431 cells were seeded in a 24-well plate as described previously. On the day of the experiment, tylocrebrine-loaded nanoparticles, dispersed in serum-free media, were added to the cells (100 μg of nanoparticles/mL). After 1 h, the media was aspirated, and the cells were washed thrice with cold 1X PBS. The cells were then lysed with 0.1 mL of RIPA buffer for 15 min. The cell lysate was divided into two parts. One part (20 μL) was analyzed by BCA assay to determine the amount of cell protein. The other part (80 μL) was extracted with a mixture of methanol and acetic acid (95:5 v/v). Tylocrebrine concentration in the methanolic extract was determined using HPLC.

***In Vitro* Efficacy of Various Formulations of Tylocrebrine.** We compared the tumor cell kill efficacy of free drug, nontargeted, and targeted nanoparticles in both neutral and acidic media. A549 cells or A431 cells were seeded in a 96-well plate (8×10^3 cells/well) and allowed to attach overnight. Nanoparticles or free drug were dispersed in serum-free RPMI media to form a stock solution. This stock solution was then diluted with either neutral or acidified serum-free media and added to the cells at various dilutions. The treatments were removed 6 h later, and the cells were washed with cold 1X PBS. The cells were then incubated with serum containing media for further 90 h. Cell viability was measured using CellTiter 96 AQ_{ueous} One Solution Cell Proliferation Assay kit (Promega, Madison, WI) according to the supplier's protocol.

Pharmacokinetics and Biodistribution of Various Formulations of Tylocrebrine. All the animal studies described here were approved by the University of Minnesota's institutional animal care and use committee.

We determined the pharmacokinetics of tylocrebrine in a mouse tumor model. A431 cells ($1-2 \times 10^6$) were dispersed in 0.05 mL of 1X PBS and injected subcutaneously in female athymic nude mice (4–6 weeks old, Taconic Biosciences, Hudson, NY). The tumors were allowed to grow to a volume of ~300 mm^3. Mice were lightly anesthetized using isofluorane and treated with various formulations of tylocrebrine (dose, 12 mg/kg; dosing volume, 10 mL/kg) via retroorbital injection.

The free drug formulation was prepared by dissolving the drug in 1 M HCl (1:1 molar ratio) and diluting the solution with saline. Excess acid was neutralized with 1 M NaOH to obtain a final drug concentration of 1.2 mg/mL. To prepare nanoparticle treatments, nanoparticles were dispersed in saline and probe sonicated at an output of 18–21 W thrice for 30 s each on an ice bath. The nanoparticle dispersion was centrifuged (1000 rpm, 5 min) to remove any large aggregates, and the supernatant was used.

At various time points, cohorts of mice were sacrificed, and blood was collected by cardiac stick. Key organs and the tumor were excised. Tissues were homogenized in ~1 mL of deionized water and lyophilized. The dry organs were then extracted overnight with a mixture of methanol and acetic acid (95:5). The extract was separated by centrifugation and dried under N_2 gas. The dried residue was redispersed in a mixture of acetonitrile and acetic acid (95:5). The resulting suspension was centrifuged (14 000 rpm, 15 min, 4 °C), and the supernatant was used for LC–MS/MS analysis.

LC–MS/MS was performed using an Acquity ultra-performance liquid chromatography (UPLC) system equipped with a Waters/Micromass Quattro Ultima mass spectrometer. LC was performed using Agilent XDB-C18 column (4.6 mm × 50 mm, 1.8 μm) as the stationary phase. A mixture of 10 mM ammonium acetate with 0.06% v/v acetic acid and acetonitrile (55:45 v/v) was used as the mobile phase. The flow rate was 0.4 mL/min, and the run time was set to 6 min. The mass spectrometer was run in the electrospray positive mode. The mass spectrometer conditions were as follows: cone voltage, 50 V; collision voltage, 20 V; dwell time, 0.4 s. Tylocrebrine was detected by monitoring the m/z transition of 394 → 324.9.

Concentration of tylocrebrine was normalized to tissue weight and injected dose and was represented as % injected dose (ID)/g of organ weight. Drug exposure in each tissue was determined by calculating the area under the concentration curve (AUC). AUC was calculated using the trapezoidal rule. The relative benefit of using the nanoparticulate formulation over the free drug was determined using the drug targeting index (DTI).[19] The DTI was calculated as shown below:

$$DTI = \frac{\left(\frac{AUC_{tumor}}{AUC_{brain}}\right)_{nanoparticle}}{\left(\frac{AUC_{tumor}}{AUC_{brain}}\right)_{freedrug}}$$

Tumor Inhibition Studies. The therapeutic efficacy of various formulations of tylocrebrine was determined in a mouse model of epidermoid cancer. About 1×10^6 A431 cells, suspended in 50 μL of 1X PBS, were injected subcutaneously in female nude mice. The dimensions of the tumor were measured periodically using a digital caliper. Tumor volume was calculated as $0.5 \times length \times width^2$. When tumor volume reached ~75 mm^3, animals were treated with saline, free drug, nontargeted nanoparticles, or EGFR-targeted nanoparticles (three doses, every 96 h, 12 mg/kg). The treatments were prepared and administered as described in the biodistribution study.

At the end of the study, animals were sacrificed, and the tumors were excised. The tumors were fixed using 5% formalin solution in 1X PBS for 24 h. After the initial fixation, tumors were

DOI: 10.1021/acs.molpharmaceut.5b00173
Mol. Pharmaceutics 2015, 12, 2912–2923

preserved in 70% ethanol. Microtome sectioning was performed on the fixed and mounted tumor samples, and the sections were stained for cleaved caspase 3 (to determine apoptosis) and Ki67 (as a marker of proliferation). Staining of tumor sections was quantified using ImageJ 1.48v software. To determine apoptotic and proliferative indices, the fraction of the total cellular area that stained positive for the individual markers was determined and presented as apoptotic and proliferative indices.

Statistical Analysis. All statistical analyses were performed using one-way analysis of variance (ANOVA) and posthoc Tukey test. For the efficacy study, a linear model was fit to log transformed tumor values. Slopes of the tumor growth profile were analyzed at each time point for each animal. One-way ANOVA and posthoc Tukey test were performed to determine if the differences in various treatments were statistically significant. A P-value < 0.05 was considered statistically significant.

RESULTS

Effect of Extracellular pH on the Cell Uptake of Tylocrebrine. Tumors are often characterized by increased production of lactic acid due to the Warburg effect.[20] Impaired drainage of the acid from the tumor microenvironment leads to low extracellular pH in the tumor.[21] Tylocrebrine is a weak base and is ionized under acidic conditions. Ionization of the drug molecule can decrease its diffusion across the cell membrane and hence lead to decreased intracellular drug availability.[22] We measured the effect of extracellular pH on drug accumulation in A431 cells (Figure 1). Decreasing the pH of the media from 7.4 (physiologic) to 6.3–6.7 (to mimic tumor microenvironment) resulted in reduced drug uptake (~60% reduction). This is likely due to the protonation of the indolizidine nitrogen, leading to a positive charge on the molecule.[23]

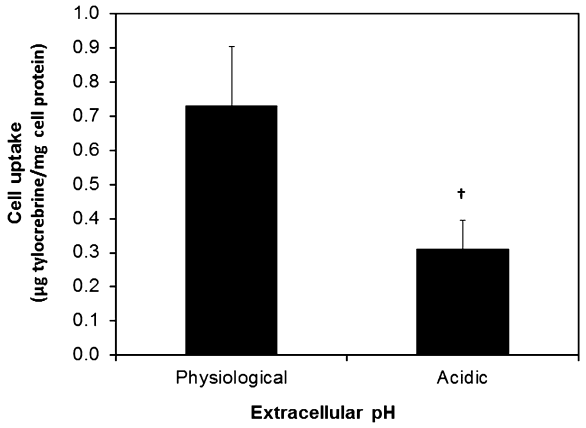

Figure 1. Effect of extracellular pH on cellular accumulation of tylocrebrine. Tylocrebrine (as free drug) was incubated with A431 cells at an extracellular pH of 7.4 (physiological) or ~6.5 (acidic). Cellular accumulation was measured by determining intracellular tylocrebrine concentration using HPLC. Tylocrebrine concentration was normalized to cell protein content. Data represented as mean ± SD, $n = 6$, † indicates $p < 0.005$.

To overcome this unfavorable ionization of tylocrebrine and reduced availability inside the cells, we formulated the drug in EGFR-targeted polymeric nanoparticles. Nanoparticles loaded with tylocrebrine and surface functionalized with PEG-COOH were first fabricated using the interfacial activity assisted surface functionalization (IAASF) technique. These nanoparticles were then conjugated to either the EGFR-targeting peptide or a control, nontargeting peptide.

Synthesis and NMR Analysis of Block Copolymer. PLA–PEG-COOH block copolymer was used to incorporate carboxyl groups on the surface of PLGA nanoparticles. We synthesized PLA–PEG-COOH through a two-step reaction involving the generation of PLA–PEG-NH_2 from PEG-NH_2 followed by the reaction of the terminal amino group with succinic anhydride. The NMR spectra of PEG-NH_2, PLA–PEG-NH_2, and PLA–PEG-COOH are shown in Figure 2. Conjugation of lactide to PEG was confirmed by the appearance of peaks at δ = 5.3 ppm and δ = 1.6 ppm.[24] Conjugation of succinate moiety to PLA–PEG-NH_2 was confirmed by the appearance of a peak at δ = 2.6 ppm.[13] On the basis of the AUC of the peaks, the molecular weight of PLA was estimated to be ~15 kDa.

Physicochemical Characterization of Nanoparticles. We initially determined the effect of reaction time on drug loading in nanoparticles and efficiency of targeting peptide conjugation to the surface of nanoparticles. Increasing the reaction time resulted in an increase in peptide conjugation efficiency but resulted in decreased drug loading (Figure 3). Particle size and zeta potential were unaffected by the duration of the reaction time. In general, the particle size was found to be in the range of 300–400 nm, and the particles had a net negative zeta potential (Table 1). We used an intermediate reaction time (5 h) for achieving optimum drug loading and conjugation efficiency. The drug and peptide loading for nanoparticles used in the rest of the studies are summarized in Table 1.

The drug release profile from nanoparticles at physiological pH is shown in Figure 4, panel A. Both targeted and nontargeted nanoparticle formulations showed a characteristic initial burst release followed by sustained release over a period of 48 h. Drug release profiles were comparable for both targeted and nontargeted nanoparticles.

Drug release from nanoparticles was also determined at pH 6.5 (Figure 4B). Drug release profiles were comparable to those obtained at physiological pH. However, the extent of burst release in acidic pH was higher than that at physiologic pH (~25% vs ~50%).

Cellular Uptake of Tylocrebrine-Loaded Nanoparticles. By using fluorescent dye labeled particles, we first determined if cellular uptake of targeted nanoparticles was greater than that of nontargeted nanoparticles. We found that targeted nanoparticles resulted in ~2–3-fold higher uptake than nontargeted nanoparticles. Additionally, uptake of targeted nanoparticles was reduced (not statistically significant) in the presence of excess free targeting peptide (Figure 5A). This indicated that the enhanced uptake of targeted nanoparticles could be mediated via EGFR. Additional experiments investigating uptake in EGFR knockout cells are needed to confirm this finding.

We determined the uptake of targeted and nontargeted tylocrebrine nanoparticles in A431 cells (Figure 5B). We found that encapsulation of tylocrebrine in targeted nanoparticles increased the cellular drug uptake by about three-fold ($p < 0.05$).

***In Vitro* Efficacy of Various Formulations of Tylocrebrine.** We compared the *in vitro* efficacy of various formulations of tylocrebrine in both A549 and A431 cells. Since our previous results showed that acidic pH led to a decreased intracellular accumulation of tylocrebrine, we performed these studies under both physiologic as well as acidic pH conditions. The free drug was found to be potent in both cell lines under neutral conditions, with IC50 values of 210 and 37 nM (Figure 6A,C).

DOI: 10.1021/acs.molpharmaceut.5b00173
Mol. Pharmaceutics 2015, 12, 2912–2923

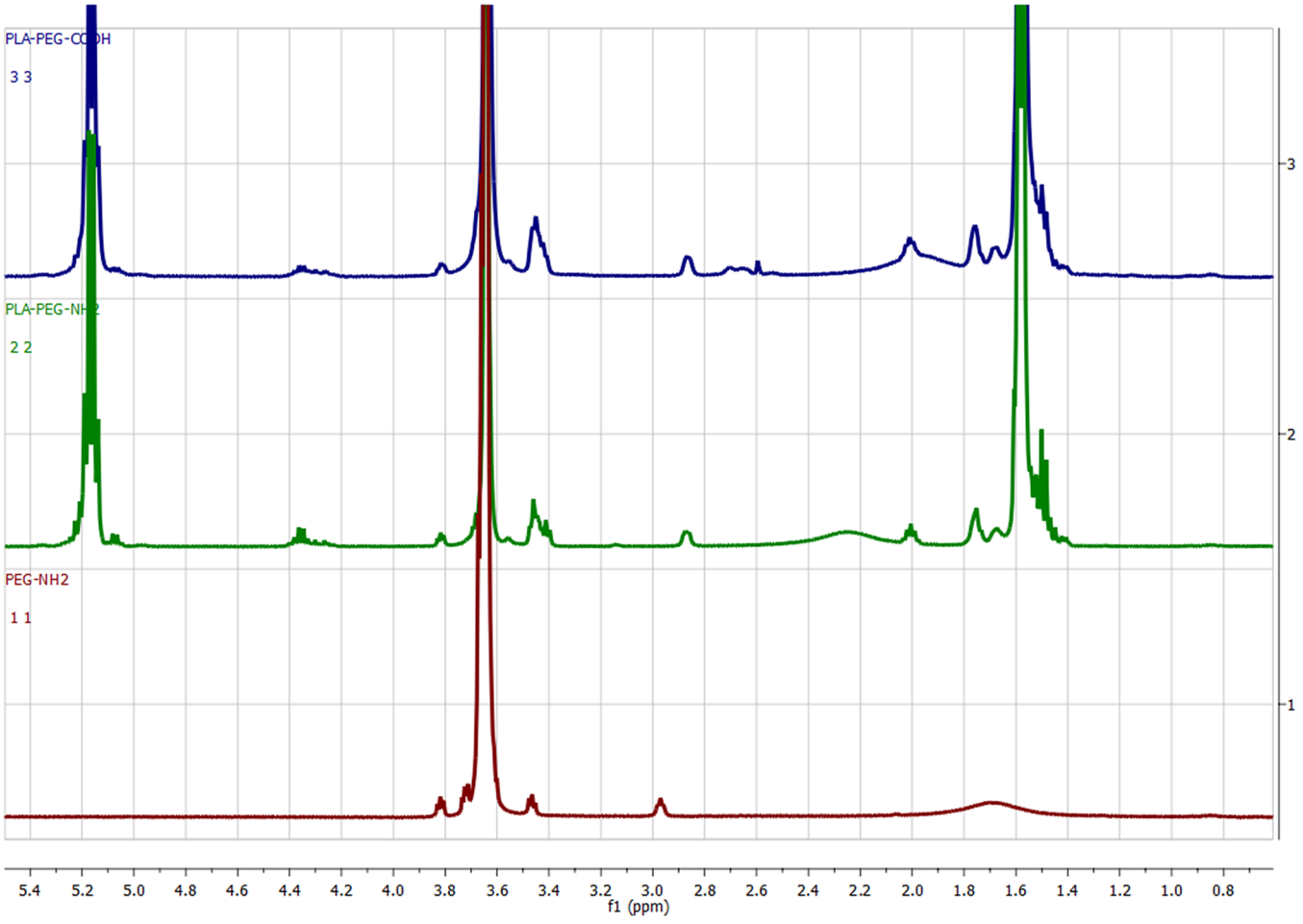

Figure 2. ^{1}H NMR spectra of PLA−PEG block copolymers. Block copolymer of PLA and carboxyl-terminated PEG were synthesized by a two-step procedure. The starting material (PEG), intermediate product (PLA−PEG-NH_2), and final product (PLA−PEG-COOH) were dissolved in deuterated chloroform and analyzed by ^{1}H NMR. Conjugation of lactide to PEG was confirmed by the appearance of peaks at 1.6 and 5.2 ppm. Conjugation of succinate to the terminal amine group in PEG was confirmed by appearance of a peak at 2.6 ppm.

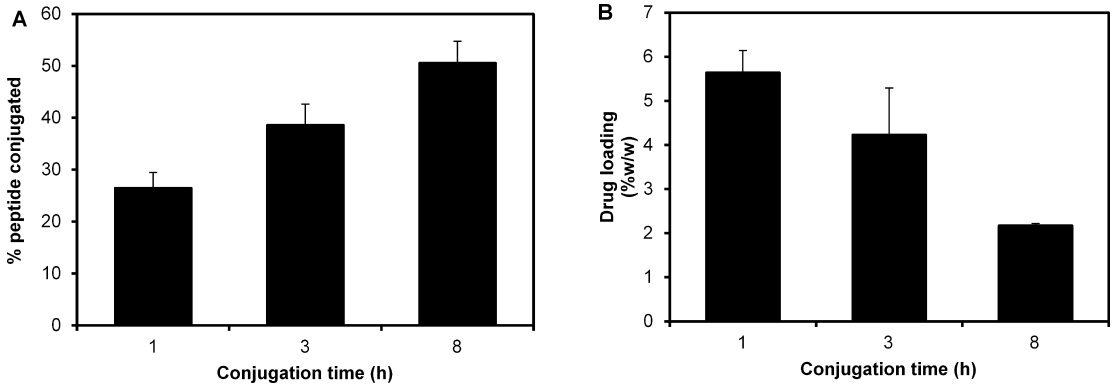

Figure 3. Effect of conjugation time on targeting peptide conjugation efficiency and drug loading. EGFR-targeting peptide was conjugated to the surface of nanoparticles using NHS−EDC chemistry. The influence of reaction time on (A) conjugation efficiency of the peptide and (B) drug loading is shown. Data represented as mean ± SD, n = 3.

However, there was a dramatic decrease in the efficacy of tylocrebrine under acidic conditions (compare Figure 6A,B and 6C,D). The IC50 values of tylocrebrine increased from 210 nM and 37 nM to 432 nM and 361 nM, respectively. At physiological pH, the efficacy of nontargeted tylocrebrine nanoparticles was comparable to that of the free drug, while targeted tylocrebrine nanoparticles were more effective than the free drug. With a decrease in extracellular pH, the IC50 value of nanoparticle formulations remained unchanged in A431 cells, while there was a small increase in IC50 for the nanoparticle formulations in A549 cells. As a result, both nontargeted and targeted tylocrebrine nanoparticles showed superior efficacy than the free drug under acidic conditions. The IC50 values estimated from the efficacy studies are summarized in Table 2.

DOI: 10.1021/acs.molpharmaceut.5b00173
Mol. Pharmaceutics 2015, 12, 2912−2923

Table 1. Physicochemical Characterization of Nanoparticles. Data Represented as Mean ± SEM, $n = 3-6$

	nontargeted nanoparticles	targeted nanoparticles
particle size (nm)	322.6 ± 34.6	365.3 ± 18.8
polydispersity index	0.17 ± 0.01	0.17 ± 0.01
zeta potential (mV)	−15.78 ± 1.15	−14.87 ± 3.46
drug loading (% w/w)	5.65 ± 0.59	5.78 ± 0.55
peptide loading (μg protein/mg nanoparticle)	9.2 ± 0.8	16.6 ± 1.4

Pharmacokinetics of Various Formulations of Tylocrebrine. Concentration−time profile of the drug in the tumor is shown in Figure 7, panel A. Accumulation of the drug and targeted nanoparticles in the tumor was rapid and reached a peak at 0.5 h. When encapsulated in nontargeted nanoparticles, tumor accumulation was slower, reaching a peak at ∼2 h. At 0.5, 2, 4, and 6 h postdose, tumor tylocrebrine concentrations in targeted nanoparticle treated group were 2−4-fold higher than free drug group. Tumor concentration of tylocrebrine in animals treated with nontargeted nanoparticles was two-fold higher than the free drug-treated animals only at 2 and 4 h postdose; the concentrations were similar to those of the free drug treatment group at later time points. AUCs of the free drug and nontargeted nanoparticles in the tumor were comparable. The AUC of targeted nanoparticles was about three-fold higher than that of the other formulations (Table 3).

The concentration−time profile of the drug in the brain (the major site of toxicity) is shown in Figure 7, panel B. Similar to that in the tumor, there was a rapid accumulation of the drug in the brain. However, encapsulation in nanoparticles resulted in a five-fold decrease in brain concentration of the drug at the first time point. Drug concentrations in the brain declined rapidly. Overall, animals treated with free drug had a two-fold higher drug exposure in the brain as compared to those treated with the nanoparticle formulations (Table 3). Targeted nanoparticles had a DTI value of ∼5 because of the reduced brain exposure and enhanced tumor exposure.

The concentration−time profile of the drug in the blood is shown in Figure 7, panel C. Nanoparticles resulted in higher blood concentration of the drug relative to that achieved after the administration of the free drug. Concentration−time profiles of the drug in other key organs are summarized in Supplemental Figure 1 of the Supporting Information.

Tumor Inhibition Studies. We determined the antitumor efficacy of the different formulations of tylocrebrine in A431 tumor model (Figure 8). There was a reduction in tumor growth rate in animals treated with tylocrebrine solution and nontargeted nanoparticles relative to that in the saline-treated animals. Treatment with nontargeted tylocrebrine nanoparticles and tylocrebrine in solution resulted in comparable activities. In agreement with our pharmacokinetic studies, treatment with EGFR targeted tylocrebrine nanoparticles resulted in greater tumor growth inhibition than that with the other formulations.

Tumor samples were stained for Ki67 and cleaved caspase 3 to determine the proliferative and apoptotic indices, respectively. Representative micrographs of Ki67 staining are shown in Figure 9. Saline-treated animals had significantly higher $Ki67^+$ cells as compared to the other treatment groups. There was no significant difference in the staining profile of free drug and nontargeted nanoparticle treated tumors. Tumors treated with targeted nanoparticles had the lowest Ki67 staining. An opposite profile was observed for cleaved caspase 3 expression (Figure 10). Cleaved caspase 3 staining was lowest in saline-treated animals and highest in animals treated with targeted nanoparticles. Taken together, these data suggest that treatment with tylocrebrine inhibited tumor cell proliferation and induced apoptosis, with targeted nanoparticles resulting in the greatest decrease in tumor cell viability.

DISCUSSION

Tylocrebrine was originally isolated in 1962 from the North Queensland vine, *T. crebriflora*.[25] With accumulating evidence that this family of phenanthropiperidine alkaloids had anticancer properties, tylocrebrine was tested and found to be effective in several cancer models.[9] Unfortunately, there were unforeseen problems with the drug, and clinical trials were terminated before tylocrebrine's therapeutic efficacy could be established in the clinic.[8] CNS toxicity, as evidenced by ataxia and disorientation, was considered the major reason for abandoning clinical trials. In the decades that followed tylocrebrine's failure in the clinic, medical interest in tylocrebrine and other members of its class waned. Recently, however, there has been a resurgence of activity with regard to these natural products and their analogs. Many of these alkaloids have been found to possess potent and broad spectrum cytotoxicity. Several members of this class, including tylocrebrine, were found to inhibit tumor cell growth with GI50 values in the low nanomolar to subnanomolar range across the NCI 60 cell line panel.[26]

A major barrier to the clinical use of tylocrebrine and other members of its class is their neurological side effects.[27] In a

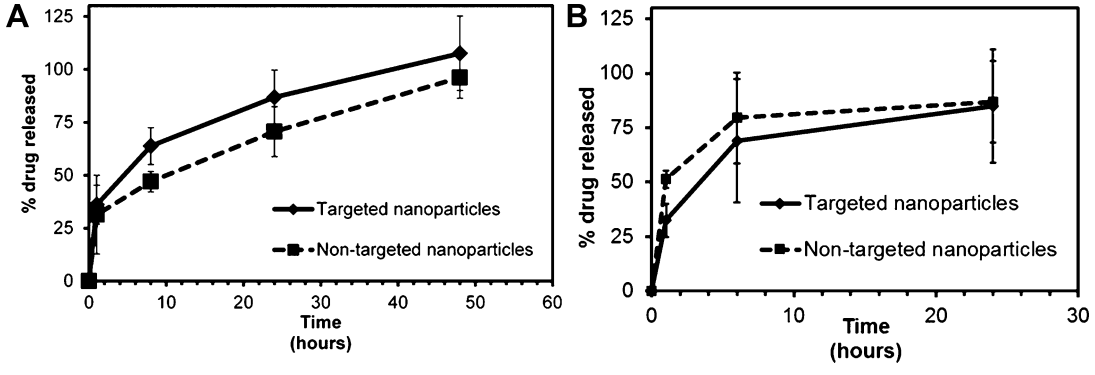

Figure 4. Drug release kinetics from tylocrebrine nanoparticles. Nanoparticles were dispersed in (A) 1X PBS (pH 7.4) or (B) 1X PBS (pH 6.5) and incubated at 37 °C and 100 rpm. Drug release from nanoparticles was monitored by analyzing tylocrebrine concentration in the release buffer using HPLC. Data represented as mean ± SD, $n = 3$.

DOI: 10.1021/acs.molpharmaceut.5b00173
Mol. Pharmaceutics 2015, 12, 2912−2923

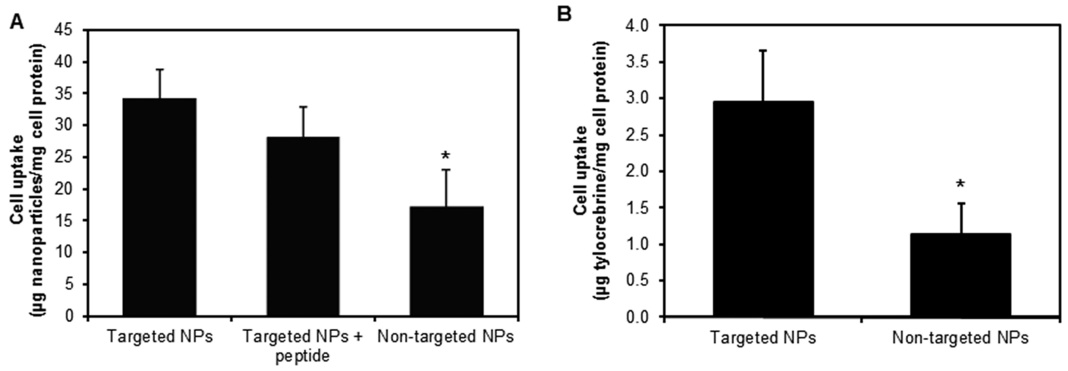

Figure 5. Cell uptake of EGFR-targeted and nontargeted nanoparticles. (A) A549 cells were incubated with coumarin 6 loaded targeted nanoparticles with or without excess peptide, or nontargeted nanoparticles for 1 h at 4 °C. Treatments were removed, and the cells were incubated in fresh media at 37 °C for 1 h. Intracellular levels of coumarin 6 were estimated using HPLC. (B) A431 cells were incubated with tylocrebrine-loaded nanoparticles. After 1 h, treatments were removed, and the cells were washed. Intracellular tylocrebrine concentration was measured using HPLC and normalized to cell protein. Data represented as mean ± SD, $n = 6$, ∗ indicates $p < 0.05$.

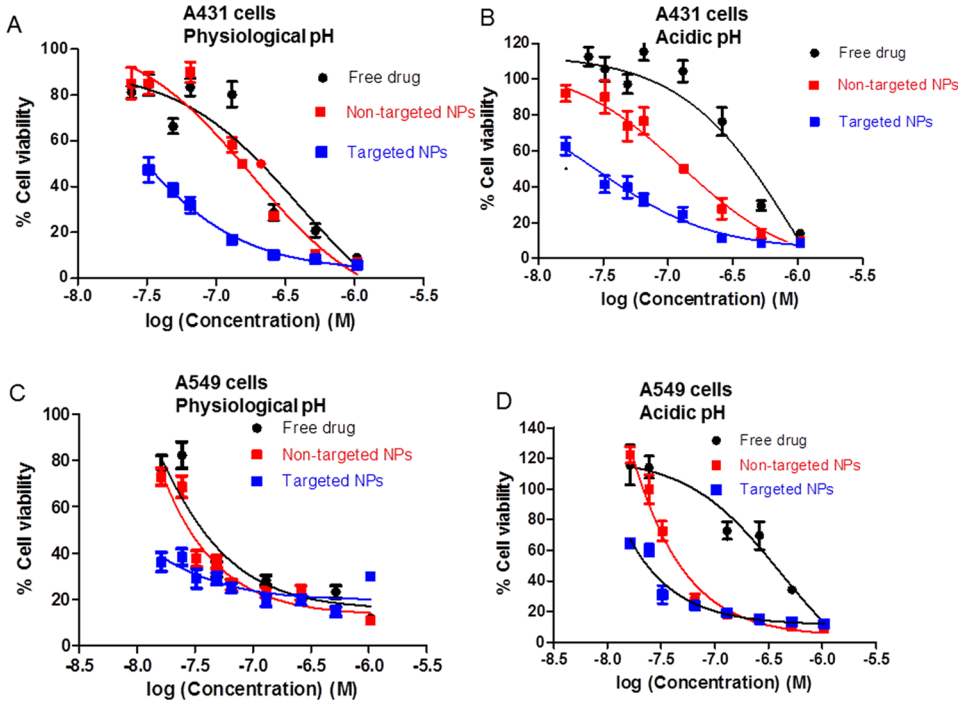

Figure 6. *In vitro* cytotoxicity of tylocrebrine. A431 and A549 cells were treated with different formulations of tylocrebrine at physiological and acidic extracellular pH. Cell viability was measured using MTS assay and normalized to untreated controls. Data represented as mean ± SD, $n = 4$.

Table 2. IC50 Values of Various Formulations of Tylocrebrine in A431 and A549 Cells

A431 cells	IC50 at physiological pH (nM)	IC50 at acidic pH (nM)
free drug	210	432
nontargeted nanoparticles	154	132
targeted nanoparticles	31	28
A549 cells	**IC50 at physiological pH (nM)**	**IC50 at acidic pH (nM)**
free drug	37	361
nontargeted nanoparticles	28	47
targeted nanoparticles	7	24

review,[28] Hitchcock and Pennington show that the degree of passive diffusion across the blood−brain barrier (BBB) correlates with a molecule's polar surface area (PSA), number of H-bond donors (HBD), cLogP, cLogD, and molecular weight.[28] A calculation of these properties for tylocrebrine reveals that each of these values is well within the suggested parameters for CNS penetrant drugs (Table 4). Increasing the hydrophilicity of tylocrebrine can potentially decrease its diffusion across the BBB. To this effect, Lee and colleagues recently reported water-soluble phenanthrene based tylophorine derivatives.[29−31] These molecules showed promising anticancer activity *in vivo* with minimal gross toxicity.[32] However, brain penetration of these molecules needs further investigation.

Tylocrebrine's anticancer activity is mediated through inhibition of protein synthesis. This effect is facilitated through binding of the drug to the 40S and 80S ribosomal subunits.[33] Hence, cellular internalization is required for its anticancer activity. Tylocrebrine is a weak base and is mainly unionized at physiological pH. Because of its neutral charge and high hydrophobicity, tylocrebrine can cross cell membranes efficiently under physiological conditions (for example, the BBB).

DOI: 10.1021/acs.molpharmaceut.5b00173
Mol. Pharmaceutics 2015, 12, 2912−2923

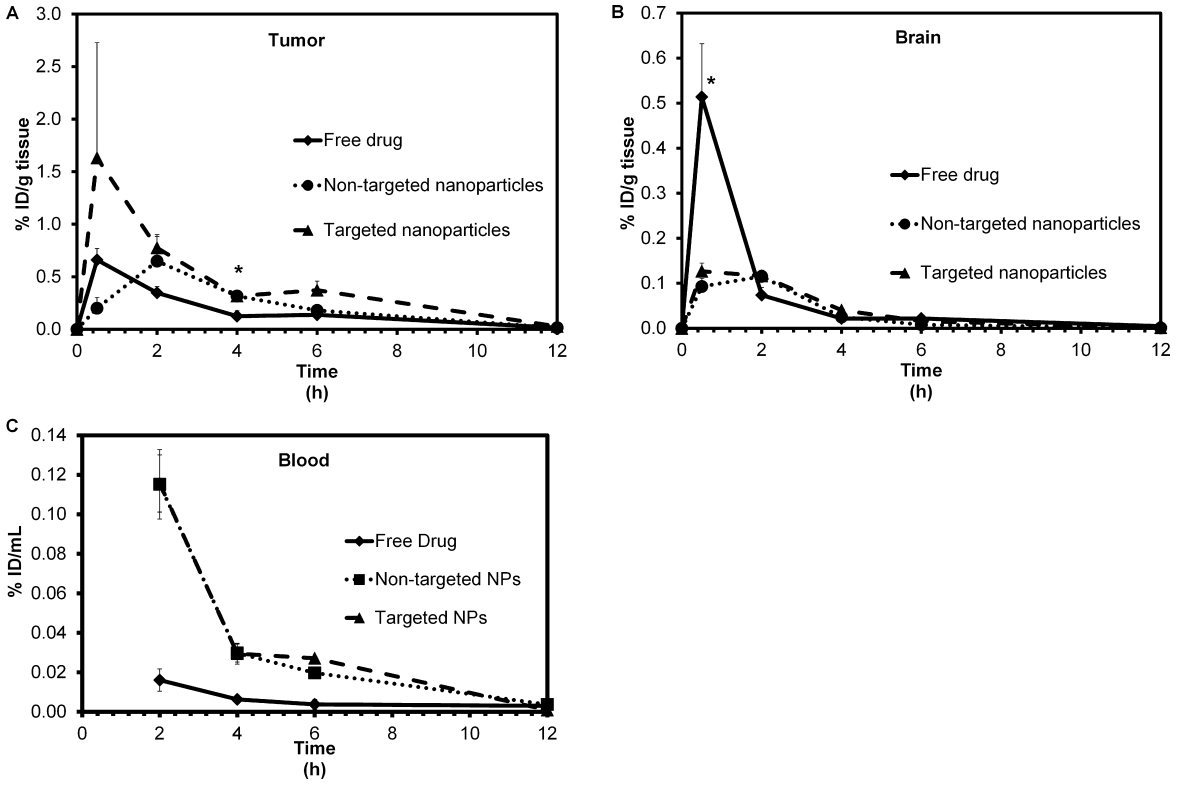

Figure 7. Pharmacokinetics of tylocrebrine. A431 tumor bearing mice were treated intravenously with tylocrebrine in solution or encapsulated in nanoparticles. At various time points, concentrations of tylocrebrine in (A) tumor, (B) brain, and (C) blood were measured using LC−MS/MS. Data represented as mean ± SEM, $n = 3–4$, ∗ indicates $p < 0.05$.

Table 3. On-Target AUC, off-Target AUC, and DTI of Tylocrebrine

	free drug	nontargeted nanoparticles	targeted nanoparticles
AUC_{tumor} (μg h mL^{-1})	5.5	6.8	17.7
AUC_{brain} (μg h mL^{-1})	2.1	1.0	1.3
DTI		2.6	5.2

However, under acidic conditions (such as those found in the tumor), tylocrebrine is ionized. This is likely to reduce its diffusion across the tumor cell membrane and its anticancer activity.

To address these twin problems of high CNS penetration and limited tumor cell uptake, we encapsulated tylocrebrine in PLGA nanoparticles surface functionalized with a peptide targeting the EGFR. PLGA nanoparticles, likely due to their colloidal size range, do not cross the intact BBB. Additionally, PLGA nanoparticles are rapidly taken up by cells through endocytosis,[34] a process augmented by the presence of targeting ligands.[35,36]

Our *in vitro* studies showed that tylocrebrine had potent activity with IC50 values in the nanomolar range. Encapsulation in EGFR-targeted nanoparticles further increased its potency. Under acidic conditions, there was a dramatic decrease in the potency of the free drug, while the activity of the nanoparticle formulations showed a minor decrease. This suggested that the issue of drug delivery into the tumor cells could be addressed through nanoparticle encapsulation. The minor decrease in the efficacy of the nanoparticle formulations can be attributed to the increase in the burst release observed in acidic pH.

Upon IV administration, we found that there was rapid accumulation of tylocrebrine in both the target tissue (tumor) and the site of toxicity (brain). Encapsulation of tylocrebrine in

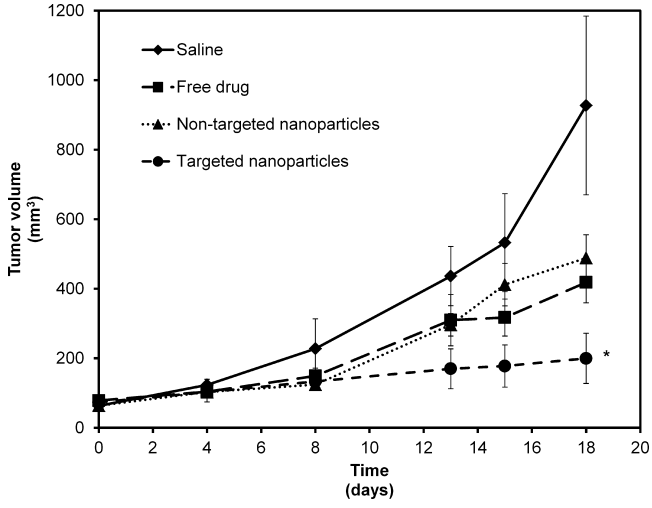

Figure 8. *In vivo* tumor inhibition studies. Antitumor efficacy of various formulations of tylocrebrine was determined in mouse A431 tumor model. Tumor bearing mice were treated with three doses of tylocrebrine (12 mg/kg) administered at 96 h intervals. Tumor volume was measured using a digital caliper. Data represented as mean ± SEM, $n = 3–4$. ∗ indicates $p < 0.05$ for saline versus targeted nanoparticles and nontargeted nanoparticles versus targeted nanoparticles.

nontargeted nanoparticles reduced the brain exposure but did not significantly improve the tumor exposure. On the other hand, delivering tylocrebrine in targeted nanoparticles resulted in both reduced brain exposure and improved tumor exposure. Our studies highlight a few important points. Use of a targeting moiety on the nanoparticle surface merely improves their accumulation at the target site without affecting their accumulation at

DOI: 10.1021/acs.molpharmaceut.5b00173
Mol. Pharmaceutics 2015, 12, 2912−2923

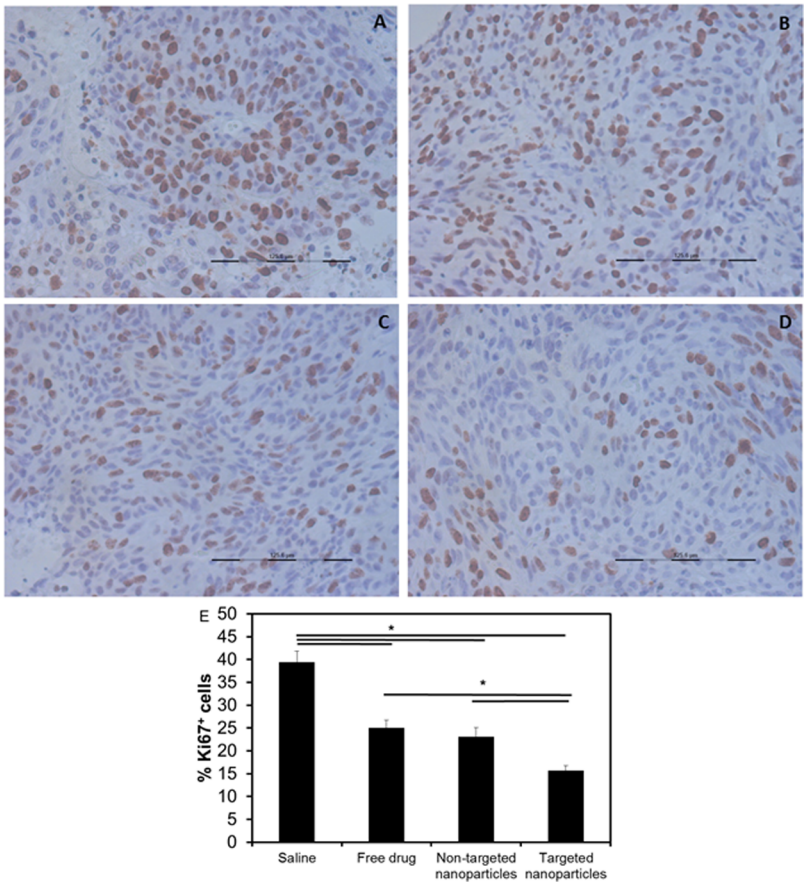

Figure 9. Ki67 staining in tumor sections. Tumors were excised at the end of the efficacy study and stained for Ki67. Representative micrographs of tumor from animals treated with (A) saline, (B) free drug, (C) nontargeted nanoparticles, and (D) targeted nanoparticles are shown. (E) Quantification of Ki67 staining. Data represented as mean ± SEM, $n = 6$ sections × 3 images/section. ∗ indicates $p < 0.05$.

nontarget sites.[37] Usually, the target site has negligible influence on the overall pharmacokinetics of the drug or drug carrier. There is still some debate in literature regarding whether targeting ligands improve the tumor accumulation of nanoparticles or merely increase their tumor cell uptake.[38] Bartlett et al. and Choi et al. have shown that transferrin receptor targeted nanoparticles have similar tumor accumulation to nontargeted nanoparticles.[39,40] However, owing to improved tumor cell uptake, these nanoparticles resulted in better efficacy. On the other hand, studies from our and other laboratories have shown that nanoparticles targeting folic acid receptor, biotin receptor, or EGFR improved tumor accumulation of encapsulated drug relative to that with nontargeted nanoparticles.[12,36,41,42] Differences in tumor models, receptor expression levels, recycling rates of different receptors, and affinities of targeting moieties could contribute to these discrepancies. Other variables such as choice of the drug, drug release kinetics and mechanisms, and plasma kinetics of drug and drug carrier also make comparison between studies difficult. Finally, current characterization techniques cannot distinguish between nanoparticle-encapsulated and free drug. Additional, in-depth characterization studies are needed to draw strong mechanistic conclusions.

Blood concentrations of nanoparticle-encapsulated tylocrebrine were significantly higher than the free drug (about six-fold higher). This indicates that the driving force for accumulation of tylocrebrine in tumors is much higher when administered in the form of nanoparticles. However, the increase in tumor levels of tylocrebrine was less dramatic (only about three-fold with targeted nanoparticles). This may be attributed to the favorable partition coefficient of the free drug into the tumor, as illustrated by a high tumor to blood concentration ratio (>10). Thus, the advantage gained by nanoencapsulation strongly depends on the drug being investigated.[19,43] Additionally, A431 tumors were found to be fluid-filled (not shown), suggesting that the interstitial fluid pressure in these tumors is high, as previously reported.[44,45] High interstitial fluid pressure (IFP) is likely to affect the intratumoral transport of nanoparticles more significantly than that of free drug molecules.[46,47] The relatively large hydrodynamic particle size of the nanoparticles used in our studies may also decrease their tumor penetration. Decreasing the particle size can potentially increase the delivery of nanoparticles into the tumor.[43,48] Alternately, tumors with a low IFP may prove to be better candidates for treatment with these formulations.

The *in vivo* tumor growth inhibition studies show that free drug inhibited tumor growth even at the low dose used. While treatment efficacy did not improve with nontargeted nanoparticles, targeted nanoparticles resulted in a considerably greater tumor growth inhibition than other treatments. This effect may be a manifestation of both the higher tumor tissue accumulation and higher cytotoxicity of targeted nanoparticles.

The dose of tylocrebrine used in our studies was relatively low (12 mg/kg). This dose was effective only if the treatment was started before the tumors reached a volume of ∼75 mm^3. Larger tumors did not respond to this dose of tylocrebrine in any formulation (data not shown). The overall dose of tylocrebrine that could be administered was limited by its loading in

DOI: 10.1021/acs.molpharmaceut.5b00173
Mol. Pharmaceutics 2015, 12, 2912−2923

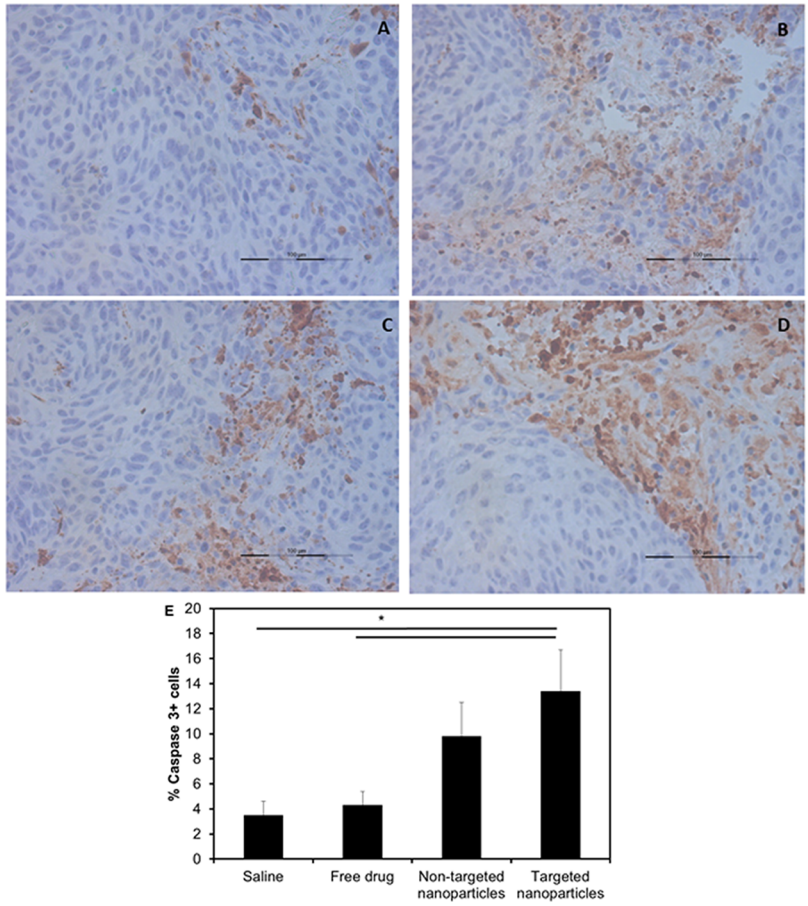

Figure 10. Cleaved caspase 3 staining in tumor sections. Micrographs of cleaved caspase 3 staining in tumors from animals treated with (A) saline, (B) free drug, (C) nontargeted nanoparticles, and (D) targeted nanoparticles are shown. (E) Quantification of staining. Data represented as mean ± SEM, n = 6 sections × 3 images/section. ∗ indicates $p < 0.05$.

Table 4. Physicochemical Characteristics of CNS Penetrant Drugs and Tylocrebrine. Mean Values and Suggested Limits Adapted with Permission from Ref 28. © 2006 American Chemical Society

property	top 25 CNS drugs mean values	suggested limits	tylocrebrine
PSA (Å^2)	47	<90	40
HBD	0.8	<3	0
cLogP	2.8	2−5	4.3
MW	293	<500	394

nanoparticles. Additionally, burst release of drug from nanoparticles may limit the overall efficiency of targeting and chemotherapeutic efficacy of nanoparticles. Strategies that enable higher drug loading and prolonged drug release will allow for larger doses to be administered, and this could further enhance the antitumor efficacy of the drug. Using polymers that have greater interaction with the drug can help achieve this goal. To this end, micelles formed from polymers consisting of aromatic rings have been shown to improve drug loading and stability as compared to micelles formed from aliphatic polymers.[49,50] This has been attributed to the formation of $\pi-\pi$ stacks between the drug and polymer. Future studies could investigate the use of such polymers for improving the therapeutic index of tylocrebrine.

CONCLUSION

Tylocrebrine is a potent anticancer agent, but significant penetration into the brain and low tumor cell uptake limit its use. Encapsulation of the drug in PLGA nanoparticles significantly limited its CNS penetration. Moreover, surface functionalizing nanoparticles with an EGFR targeting peptide led to enhanced tumor cell uptake, tumor tissue accumulation, and *in vivo* antitumor efficacy. We expect that the reformulation approach presented here will enable further clinical testing of a number of previously abandoned drug candidates while potentially minimizing drug development costs.

ASSOCIATED CONTENT

Supporting Information

Concentration−time profiles of the drug in other key organs. The Supporting Information is available free of charge on the ACS Publications website at DOI: 10.1021/acs.molpharmaceut.5b00173.

AUTHOR INFORMATION

Corresponding Author

*Phone: 612-624-0951. Fax: 612-626-2125. E-mail: jpanyam@umn.edu.

Author Contributions

The manuscript was written through contributions of all authors. All authors have given approval to the final version of the manuscript.

Notes

The authors declare no competing financial interest.

DOI: 10.1021/acs.molpharmaceut.5b00173
Mol. Pharmaceutics 2015, 12, 2912−2923

■ ACKNOWLEDGMENTS

The authors thank James Fisher (Clinical Pharmacology Analytical Services, UMN) for assistance with LC−MS/MS, and Comparative Pathology Core for preparation of immunohistochemistry slides. The authors also thank Charles River Discovery Services for preliminary animal studies. Funding from Frederick National Laboratory for Cancer Research (11XS245) and from the University of Minnesota. This work was also supported in part by NIH P30 CA77598 and Minnesota Masonic Charities.

■ ABBREVIATIONS

CNS, central nervous system; EGFR, epidermal growth factor receptor; PLGA, poly(lactide-*co*-glycolide); EPR, enhanced permeability and retention; BCA, bicinchoninic acid assay; RIPA, radioimmunoprecipitation assay; PLA, poly(lactide); PEG, poly(ethylene glycol); PBS, phosphate buffered saline; AUC, area under the curve; DTI, drug targeting index

■ REFERENCES

(1) Niraula, S.; Amir, E.; Vera-Badillo, F.; Seruga, B.; Ocana, A.; Tannock, I. F. Risk of Incremental Toxicities and Associated Costs of New Anticancer Drugs: A Meta-Analysis. *J. Clin. Oncol.* **2014**, *32* (32), 3634−3642.

(2) Kaitin, K. I. Deconstructing the Drug Development Process: The New Face of Innovation. *Clin. Pharmacol. Ther.* **2010**, *87* (3), 356−361.

(3) Grossman, J. H.; McNeil, S. E. *Preclinical Efficacy and Toxicity of Engineered Nanomaterials*; Karger: Basel, Switzerland, 2011; Vol. 2.

(4) Wang, A. Z. Nanoparticle Drug Delivery: Focusing on the Therapeutic Cargo. *Nanomedicine (London, U. K.)* **2012**, *7* (10), 1463−1465.

(5) Kirkpatrick, P. Pressures in the Pipeline. *Nat. Rev. Drug Discovery* **2003**, *2* (5), 337−337.

(6) Kwong, E. Advancing Drug Discovery: A Pharmaceutics Perspective. *J. Pharm. Sci.* **2015**, *104* (3), 865−871.

(7) Karve, S.; Werner, M. E.; Sukumar, R.; Cummings, N. D.; Copp, J. A.; Wang, E. C.; Li, C.; Sethi, M.; Chen, R. C.; Pacold, M. E.; Wang, A. Z. Revival of the Abandoned Therapeutic Wortmannin by Nanoparticle Drug Delivery. *Proc. Natl. Acad. Sci. U. S. A.* **2012**, *109* (21), 8230−8235.

(8) Suffness, M.; Cordell, G. A. *The Alkaloids*; Brossi, A., Ed.; Academic Press: New York, 1985; Vol. 25.

(9) Gellert, E.; Rudzats, R. The Antileukemia Activity of Tylocrebrine. *J. Med. Chem.* **1964**, *7*, 361−362.

(10) Iyer, A. K.; Khaled, G.; Fang, J.; Maeda, H. Exploiting the Enhanced Permeability and Retention Effect for Tumor Targeting. *Drug Discovery Today* **2006**, *11* (17−18), 812−818.

(11) Maeda, H.; Nakamura, H.; Fang, J. The EPR Effect for Macromolecular Drug Delivery to Solid Tumors: Improvement of Tumor Uptake, Lowering of Systemic Toxicity, and Distinct Tumor Imaging *in Vivo*. *Adv. Drug Delivery Rev.* **2013**, *65* (1), 71−79.

(12) Milane, L.; Duan, Z. F.; Amiji, M. Pharmacokinetics and Biodistribution of Lonidamine/Paclitaxel Loaded, EGFR-Targeted Nanoparticles in an Orthotopic Animal Model of Multidrug Resistant Breast Cancer. *Nanomedicine* **2011**, *7* (4), 435−444.

(13) Sadhukha, T.; Wiedmann, T. S.; Panyam, J. Inhalable Magnetic Nanoparticles for Targeted Hyperthermia in Lung Cancer Therapy. *Biomaterials* **2013**, *34* (21), 5163−5171.

(14) Nicholson, R. I.; Gee, J. M.; Harper, M. E. EGFR and Cancer Prognosis. *Eur. J. Cancer* **2001**, *37* (Suppl. 4), S9−S15.

(15) Niphakis, M. J.; Georg, G. I. Synthesis of Tylocrebrine and Related Phenanthroindolizidines by VOF3-Mediated Oxidative Aryl−Alkene Coupling. *Org. Lett.* **2011**, *13* (2), 196−199.

(16) Qian, H.; Wohl, A. R.; Crow, J. T.; Macosko, C. W.; Hoye, T. R. A Strategy for Control of "Random" Copolymerization of Lactide and Glycolide: Application to Synthesis of PEG-b-PLGA Block Polymers Having Narrow Dispersity. *Macromolecules* **2011**, *44* (18), 7132−7140.

(17) Roger, E.; Kalscheuer, S.; Kirtane, A.; Guru, B. R.; Grill, A. E.; Whittum-Hudson, J.; Panyam, J. Folic Acid Functionalized Nanoparticles for Enhanced Oral Drug Delivery. *Mol. Pharmaceutics* **2012**, *9* (7), 2103−2110.

(18) Toti, U. S.; Guru, B. R.; Grill, A. E.; Panyam, J. Interfacial Activity Assisted Surface Functionalization: A Novel Approach To Incorporate Maleimide Functional Groups and cRGD Peptide on Polymeric Nanoparticles for Targeted Drug Delivery. *Mol. Pharmaceutics* **2010**, *7* (4), 1108−1117.

(19) Hunt, C. A.; Macgregor, R. D.; Siegel, R. A. Engineering Targeted *in Vivo* Drug Delivery. I. The Physiological and Physicochemical Principles Governing Opportunities and Limitations. *Pharm. Res.* **1986**, *3* (6), 333−344.

(20) Vander Heiden, M. G.; Cantley, L. C.; Thompson, C. B. Understanding the Warburg Effect: The Metabolic Requirements of Cell Proliferation. *Science* **2009**, *324* (5930), 1029−1033.

(21) Tannock, I. F.; Rotin, D. Acid pH in Tumors and Its Potential for Therapeutic Exploitation. *Cancer Res.* **1989**, *49* (16), 4373−4384.

(22) Raghunand, N.; Mahoney, B. P.; Gillies, R. J. Tumor Acidity, Ion Trapping, and Chemotherapeutics. II. pH-Dependent Partition Coefficients Predict Importance of Ion Trapping on Pharmacokinetics of Weakly Basic Chemotherapeutic Agents. *Biochem. Pharmacol.* **2003**, *66* (7), 1219−1229.

(23) Chemler, S. R. Phenanthroindolizidines and Phenanthroquinolizidines: Promising Alkaloids for Anticancer Therapy. *Curr. Bioact. Compd.* **2009**, *5* (1), 2−19.

(24) Ignjatovic, N.; Tomic, S.; Dakic, M.; Miljkovic, M.; Plavsic, M.; Uskokovic, D. Synthesis and Properties of Hydroxyapatite/Poly-L-lactide Composite Biomaterials. *Biomaterials* **1999**, *20* (9), 809−816.

(25) Gellert, E.; Govindachari, T. R.; Lakshmikantham, M. V.; Ragade, I. S.; Rudzats, R.; Viswanathan, N. 189. The Alkaloids of Tylophora Crebriflora: Structure and Synthesis of Tylocrebrine, a New Phenanthroindolizidine Alkaloid. *J. Chem. Soc. (Resumed)* **1962**, No. 0, 1008−1014.

(26) Lin, J.-C.; Yang, S.-C.; Hong, T.-M.; Yu, S.-L.; Shi, Q.; Wei, L.; Chen, H.-Y.; Yang, P.-C.; Lee, K.-H. Phenanthrene-Based Tylophorine-1 (PBT-1) Inhibits Lung Cancer Cell Growth through the Akt and NF-Î°B Pathways. *J. Med. Chem.* **2009**, *52* (7), 1903−1911.

(27) Gopalakrishnan, C.; S, D.; Kameswaran, L.; Natarajan, S. Pharmacological Investigations of Tylophorine, the Major Alkaloid of *Tylophora indica*. *Indian J. Med. Res.* **1979**, *69*, 513−520.

(28) Hitchcock, S. A.; Pennington, L. D. Structure−Brain Exposure Relationships. *J. Med. Chem.* **2006**, *49* (26), 7559−7583.

(29) Zhang, S.; Wei, L.; Bastow, K.; Zheng, W.; Brossi, A.; Lee, K. H.; Tropsha, A. Antitumor Agents 252. Application of Validated QSAR Models to Database Mining: Discovery of Novel Tylophorine Derivatives as Potential Anticancer Agents. *J. Comput. Aided Mol. Des.* **2007**, *21* (1−3), 97−112.

(30) Yang, X.; Shi, Q.; Liu, Y. N.; Zhao, G.; Bastow, K. F.; Lin, J. C.; Yang, S. C.; Yang, P. C.; Lee, K. H. Antitumor agents 268. Design, Synthesis, and Mechanistic Studies of New 9-Substituted Phenanthrene-Based Tylophorine Analogues as Potent Cytotoxic Agents. *J. Med. Chem.* **2009**, *52* (16), 5262−5268.

(31) Wei, L.; Brossi, A.; Kendall, R.; Bastow, K. F.; Morris-Natschke, S. L.; Shi, Q.; Lee, K. H. Antitumor Agents 251: Synthesis, Cytotoxic Evaluation, and Structure−Activity Relationship Studies of Phenanthrene-Based Tylophorine Derivatives (PBTs) as a New Class of Antitumor Agents. *Bioorg. Med. Chem.* **2006**, *14* (19), 6560−6569.

(32) Wei, L.; Shi, Q.; Bastow, K. F.; Brossi, A.; Morris-Natschke, S. L.; Nakagawa-Goto, K.; Wu, T. S.; Pan, S. L.; Teng, C. M.; Lee, K. H. Antitumor Agents 253. Design, Synthesis, and Antitumor Evaluation of Novel 9-Substituted Phenanthrene-Based Tylophorine Derivatives as Potential Anticancer Agents. *J. Med. Chem.* **2007**, *50* (15), 3674−3680.

(33) Huang, M. T.; Grollman, A. P. Mode of Action of Tylocrebrine: Effects on Protein and Nucleic Acid Synthesis. *Mol. Pharmacol.* **1972**, *8* (5), 538−550.

(34) Panyam, J.; Zhou, W. Z.; Prabha, S.; Sahoo, S. K.; Labhasetwar, V. Rapid Endo-Lysosomal Escape of Poly(DL-lactide-co-glycolide) Nano-

DOI: 10.1021/acs.molpharmaceut.5b00173
Mol. Pharmaceutics 2015, 12, 2912−2923

particles: Implications for Drug and Gene Delivery. *FASEB J.* **2002**, *16* (10), 1217−1226.
(35) Patil, Y. B.; Swaminathan, S. K.; Sadhukha, T.; Ma, L.; Panyam, J. The Use of Nanoparticle-Mediated Targeted Gene Silencing and Drug Delivery To Overcome Tumor Drug Resistance. *Biomaterials* **2010**, *31* (2), 358−365.
(36) Patil, Y. B.; Toti, U. S.; Khdair, A.; Ma, L.; Panyam, J. Single-Step Surface Functionalization of Polymeric Nanoparticles for Targeted Drug Delivery. *Biomaterials* **2009**, *30* (5), 859−866.
(37) Bae, Y. H.; Park, K. Targeted Drug Delivery to Tumors: Myths, Reality, and Possibility. *J. Controlled Release* **2011**, *153* (3), 198−205.
(38) Pirollo, K. F.; Chang, E. H. Does a Targeting Ligand Influence Nanoparticle Tumor Localization or Uptake? *Trends Biotechnol.* **2008**, *26* (10), 552−558.
(39) Bartlett, D. W.; Su, H.; Hildebrandt, I. J.; Weber, W. A.; Davis, M. E. Impact of Tumor-Specific Targeting on the Biodistribution and Efficacy of siRNA Nanoparticles Measured by Multimodality *in Vivo* Imaging. *Proc. Natl. Acad. Sci. U. S. A.* **2007**, *104* (39), 15549−15554.
(40) Choi, C. H.; Alabi, C. A.; Webster, P.; Davis, M. E. Mechanism of Active Targeting in Solid Tumors with Transferrin-Containing Gold Nanoparticles. *Proc. Natl. Acad. Sci. U. S. A.* **2010**, *107* (3), 1235−1240.
(41) Qian, X.; Peng, X. H.; Ansari, D. O.; Yin-Goen, Q.; Chen, G. Z.; Shin, D. M.; Yang, L.; Young, A. N.; Wang, M. D.; Nie, S. *In Vivo* Tumor Targeting and Spectroscopic Detection with Surface-Enhanced Raman Nanoparticle Tags. *Nat. Biotechnol.* **2008**, *26* (1), 83−90.
(42) Yang, L.; Mao, H.; Wang, Y. A.; Cao, Z.; Peng, X.; Wang, X.; Duan, H.; Ni, C.; Yuan, Q.; Adams, G.; Smith, M. Q.; Wood, W. C.; Gao, X.; Nie, S. Single Chain Epidermal Growth Factor Receptor Antibody Conjugated Nanoparticles for *in Vivo* Tumor Targeting and Imaging. *Small* **2009**, *5* (2), 235−243.
(43) Kirtane, A. R.; Siegel, R. A.; Panyam, J. A Pharmacokinetic Model for Quantifying the Effect of Vascular Permeability on the Choice of Drug Carrier: A Framework for Personalized Nanomedicine. *J. Pharm. Sci.* **2015**, *104* (3), 1174−1186.
(44) Hofmann, M.; Guschel, M.; Bernd, A.; Bereiter-Hahn, J.; Kaufmann, R.; Tandi, C.; Wiig, H.; Kippenberger, S. Lowering of Tumor Interstitial Fluid Pressure Reduces Tumor Cell Proliferation in a Xenograft Tumor Model. *Neoplasia* **2006**, *8* (2), 89−95.
(45) Torosean, S.; Flynn, B.; Axelsson, J.; Gunn, J.; Samkoe, K. S.; Hasan, T.; Doyley, M. M.; Pogue, B. W. Nanoparticle Uptake in Tumors Is Mediated by the Interplay of Vascular and Collagen Density with Interstitial Pressure. *Nanomedicine* **2013**, *9* (2), 151−158.
(46) Stylianopoulos, T.; Jain, R. K. Combining Two Strategies To Improve Perfusion and Drug Delivery in Solid Tumors. *Proc. Natl. Acad. Sci. U. S. A.* **2013**, *110* (46), 18632−18637.
(47) Kirtane, A. R.; Kalscheuer, S. M.; Panyam, J. Exploiting Nanotechnology To Overcome Tumor Drug Resistance: Challenges and Opportunities. *Adv. Drug Delivery Rev.* **2013**, *65* (13−14), 1731−1747.
(48) Cabral, H.; Matsumoto, Y.; Mizuno, K.; Chen, Q.; Murakami, M.; Kimura, M.; Terada, Y.; Kano, M. R.; Miyazono, K.; Uesaka, M.; Nishiyama, N.; Kataoka, K. Accumulation of Sub-100 nm Polymeric Micelles in Poorly Permeable Tumours Depends on Size. *Nat. Nanotechnol.* **2011**, *6* (12), 815−823.
(49) Yokoyama, M.; Fukushima, S.; Uehara, R.; Okamoto, K.; Kataoka, K.; Sakurai, Y.; Okano, T. Characterization of Physical Entrapment and Chemical Conjugation of Adriamycin in Polymeric Micelles and Their Design for *in Vivo* Delivery to a Solid Tumor. *J. Controlled Release* **1998**, *50* (1−3), 79−92.
(50) Shi, Y.; van Steenbergen, M. J.; Teunissen, E. A.; Novo, L.; Gradmann, S.; Baldus, M.; van Nostrum, C. F.; Hennink, W. E. Pi−Pi Stacking Increases the Stability and Loading Capacity of Thermosensitive Polymeric Micelles for Chemotherapeutic Drugs. *Biomacromolecules* **2013**, *14* (6), 1826−1837.

DOI: 10.1021/acs.molpharmaceut.5b00173
Mol. Pharmaceutics 2015, 12, 2912−2923